Seismic behavior of fiber reinforced cementitious composites coupling beams with conventional reinforcement

Xingwen Liang[*] and Pengtao Xing

School of Civil Engineering, Xi'an University of Architecture and Technology, No. 13 Yanta Road, Xi'an 710055, P.R. China

Abstract. Fiber reinforced cementitious composites (FRCC) materials that exhibit strain-hardening and multiple cracking properties under tension were recently developed as innovative building materials for construction. This study aims at exploring the use of FRCC on the seismic performance of coupling beams with conventional reinforcement. Experimental tests were conducted on seven FRCC precast coupling beams with small span-to-depth ratios and one ordinary concrete coupling beam for comparison. The crack and failure modes of the specimens under the low cycle reversed loading were observed, and the hysteretic characteristics, deformation capacity, energy dissipation capacity and stiffness degradation were also investigated. The results show that the FRCC coupling beams have good ductility and energy dissipation capacities compared with the ordinary concrete coupling beam. As the confinement stirrups and span-to-depth ratio increase, the deformation capacity and energy dissipation capacity of coupling beams can be improved significantly. Finally, based on the experimental analysis and shear mechanism, a formula for the shear capacity of the coupling beams with small span-to-depth ratios was also presented, and the calculated results agreed well with the experimental results.

Keywords: fiber reinforced cementitious composites; coupling beam; span-to-depth ratio; quasi-static test; conventional reinforcement; shear capacity

1. Introduction

Structural walls with coupling beams are widely used as the primary lateral load resisting system for both medium height and high-rise building structures. To ensure adequate seismic performance and to minimize the repair costs after an earthquake, coupling beams and walls must be capable of sustaining large inelastic deformations and exhibit significant damage tolerance. Because of architectural requirements, openings for doors and windows are usually created in structural walls, and the span-to-depth ratio of coupling beams is small. A coupling beam is an antisymmetrical and deep flexural beam that the nominal shear stress is relatively high. For the coupling beams with small span-to-depth ratio (the span-to-depth ratio is not greater than 2.5), it is difficult to avoid brittle shear failures in severe earthquakes, and coupling beams cannot act as the first seismic defense line.

Improvements in the seismic performance of coupling beams with small span-to-depth ratios are required so that the structure exhibits a rational failure mechanism and the coupling beams can serve as a primary source for energy dissipation when the structure is subjected to an earthquake. From the standpoint of reinforcement schemes and materials, some experimental research and theoretical analysis have been conducted. Paulay and Binney (1974) first proposed diagonal reinforcement for coupling beams.

Experimental results confirm that diagonally reinforced coupling beams have good ductility, energy dissipation capacities and stiffness retention under large displacement reversals (Paulay and Binney 1974, Tassios *et al*. 1996), and this reinforcement pattern has been adopted by the ACI Building Code (ACI 318 2014). Unfortunately, this reinforcement detailing has led to reinforcement congestion and construction difficulties. To resolve these problems, other alternatives have been investigated, such as the addition of dowels, diagonal reinforcements only at the beam-wall interface, or bundled diagonal reinforcement (Tassios *et al*. 1996, Galano and Vignoli 2000, Fortney *et al*. 2008, Han *et al*. 2015). In addition, steel and composite coupling beams were also developed (Harries *et al*. 2000, Gong 2001). Because of the limitations of reinforcement detailing of coupling beams, new alternatives have started using composite materials. Canbolat *et al*. (2005) conducted experimental studies to investigate the seismic behavior of high-performance fiber-reinforced cement composite (HPFRCC) coupling beams with different fiber types and reinforcement configurations, and the results showed that the HPFRCC provides confinement to the concrete and diagonal reinforcement and HPFRCC coupling beams with simplified diagonal reinforcement exhibited higher shear strength and stiffness retention. Park and Yun (2011) conducted experiments to investigate the seismic performance of pseudo strain-hardening cementitious composite (PSH2C) coupling beams, and the results show that PSH2C coupling beams exhibit an improved hysteretic response compared with conventional RC coupling beams. Lequesne *et al*. (2013, 2016) studied HPFRCC coupling beams and showed the use of HPFRCC provides a

---

*Corresponding author, Professor
 E-mail: liangxingwen2000@163.com

Table 1 Specimen parameters

Specimen	l_n (mm)	l_n/h	Transv. Reinf.	f_{cu} (MPa)	f_t (MPa)	Material
CB-1	600	1.0	D8@75	54.24	4.42	FRCC1
CB-2	900	1.5	D8@75	54.24	4.42	FRCC1
CB-3	1200	2.0	D8@75	54.24	4.42	FRCC1
CB-4	600	1.0	D8@75	40.62	2.56	FRCC2
CB-5	600	1.0	D8@75	60.70	4.81	FRCC3
CB-6	900	1.5	D8@50	54.24	4.42	FRCC1
CB-7	900	1.5	D8@100	54.24	4.42	FRCC1
CB-8	900	1.5	D8@75	51.09	3.44	Concrete

Note: l_n is the span of the coupling beam, h is the height of the coupling beam section, f_t is the measured tensile strength, f_{cu} is the measured cubic compressive strength.

reduction in the reinforcement required to achieve a stable coupling beam response by providing confinement and contributing to the beam shear strength.

Fiber reinforced cementitious composites (FRCC) exhibit strain-hardening response under uniaxial tension by developing numerous micro-cracks with assistance of engineered fibers. FRCC have much higher ductility and energy absorption capacity than normal concrete (Li and Kanda 1998, Kanda *et al*. 2000, Li *et al*. 2001, Fischer and Li 2002, 2003). Moreover, FRCC materials have a good ability to control the crack width when the deformation increases, which can be used in structural concrete members, such as coupling beams and beam-column connections, as well as in plastic hinge regions of beams, columns, and structural walls (Shin *et al*. 2014, Khan and Abbass 2016, Foltz *et al*. 2017). FRCC materials increase the shear strength, deformation and energy dissipation capacity as well as the damage tolerance of flexural and shear members, which can significantly improve the seismic performance and shear behavior of ordinary concrete structures. These excellent properties provide an attractive alternative for replacing concrete in these critical regions.

To improve the ductility and energy dissipation of coupling beams with a small span-to-depth ratio, FRCC materials were used in conventionally reinforced coupling beams in this study. Seven FRCC coupling beams with small span-to-depth ratios and one ordinary concrete coupling beam for comparison were designed and tested under cyclic loading. The influence of the span-to-depth ratio, stirrup spacing and the strength of FRCC materials on the seismic performance of the coupling beams was investigated, which provides a reference for the application of FRCC materials in practical engineering.

2. Experimental program

2.1 Test specimens

Seven FRCC coupling beam specimens and one RC coupling beam specimen were built and subjected to reverse cyclic displacements that increased in magnitude until failure of the specimen. The prototype of the specimens
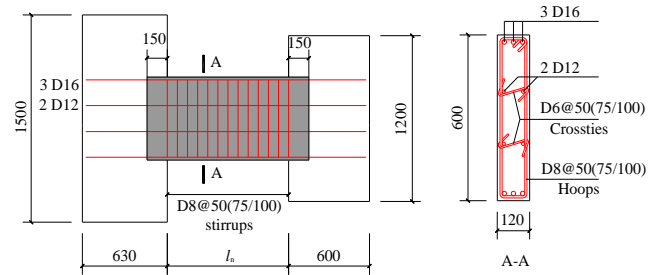

Fig. 1 Dimensions and reinforcement details of test specimens

Table 2 Mix proportions of FRCC

Material	Normalized weight			
	OPC	FA	S	W
FRCC1	1	1.22	0.8	0.8
FRCC2	1	1.5	0.9	1
FRCC3	1	1	0.9	0.64

Note: OPC: Ordinary Portland cement; FA: Fly ash (Grade I, 45 μm sieve residue ≤12%, moisture content ≤1%, loss on ignition ≤5%, water demand ratio ≤95%, content of SO_3≤ 3%); S: Silica sand (maximum size of silica sand ≤1.18 mm); W: Water. The Naphthalene series water-reducing agent is also added to ensure good workability of the mixture.

Table 3 Properties of PVA fibers

Fiber type	l_f (mm)	d_f (μm)	f_f (MPa)	E_f (GPa)	A_f (%)
PVA	12	39	1600	40	7

Note: l_f is the length of PVA fiber, d_f is the diameter of the PVA fiber, f_f is the tensile strength of PVA fiber, E_f is the Young's modulus of PVA fiber. A_f is the elongation ratio of PVA fiber.
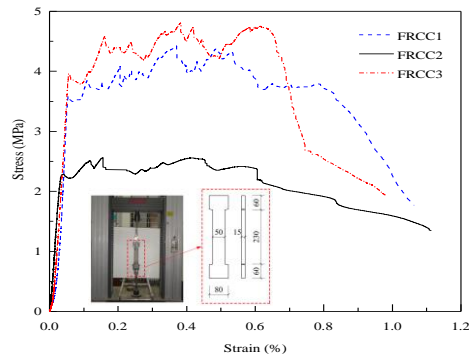
included the linking together of shear walls using coupling beams in a coupled wall system. Each specimen consisted of an approximately 1/2 scale coupling beam and two stiff RC blocks to simulate the structural wall boundary elements. The main variables include the span-to-depth ratio, stirrup ratio and the strength of FRCC. The specimen details and test variables are summarized in Table 1. The width and height of the coupling beam were 120 mm and 600 mm for all of the specimens, respectively. The dimensions and reinforcement details of the specimens are shown in Fig. 1. The reinforcements of the wall pier and coupling beam were constructed separately and then assembled together, the longitudinal bars of the coupling beam were extended into the wall for anchorage, and the transverse reinforcements were only arranged within the span of the coupling beam.

2.2 Material properties

The FRCC material is mixed using cement, fly ash, sand, water reducer, water and fiber. The mix proportions of FRCC used in this study are given in Table 2. Polyvinyl alcohol (PVA) fibers in a 2% volume fraction are used as

Table 4 Mechanical properties of steel reinforcement

Steel type	Steel grade	Diameter (mm)	Yield strength (MPa)	Ultimate strength (MPa)
D16	HRB400	16	530	710
D12	HRB400	12	475	655
D8	HPB300	8	480	520

(a) Tensile stress versus strain response

(b) Crack patterns

Fig. 2 Tensile test results of the FRCC samples

cement-based reinforced material in this study, and basic parameters are shown in Table 3. Specimen CB-8 and the wall pier of the rest of the specimens were fabricated using commercial concrete, which was provided by a local ready-mix concrete supplier. The longitudinal reinforcement of the coupling beams included 16 mm and 12 mm diameter hot-rolled ribbed bars. The transverse reinforcement of the coupling beams included 8 mm diameter hot-rolled plain bars, and the measured properties of reinforcing steel are shown in Table 4.

The compressive strength of the FRCC and concrete were determined by averaging the results of three $100 \times 100 \times 100$ mm and $150 \times 150 \times 150$ mm cubes that were fabricated using the same concrete mix and cured under the same conditions as the companion specimen, respectively. The tensile stress versus strain response and crack patterns of the FRCC materials with the PVA fibers that was obtained from the dumbbell-shaped specimens are shown in Fig. 2. The measured compressive strength and tensile strength of FRCC and concrete are reported in Table 1.

2.3 Test setup and instrumentation

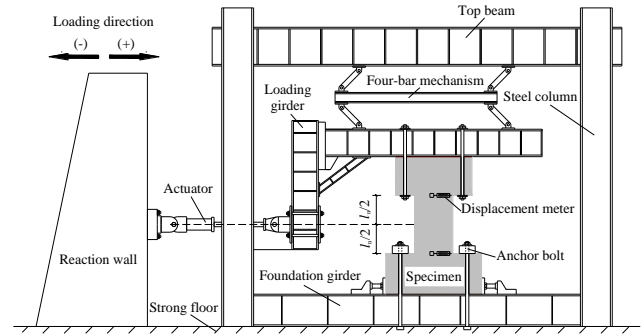A schematic diagram of the test setup is illustrated in

Fig. 3 Test setup

Fig. 3. The coupling beam specimens were rotated 90° from their actual orientation in a building for testing convenience. The lower end-block was bolted to the foundation girder to approximate a fixed boundary condition. The upper end-block was connected to the *L*-shaped loading girder using bolts. The lateral displacement was applied using a 1000 kN servo-hydraulic actuator that was made by American MTS Company with its line of action passing through the midspan of the coupling beam to produce an antisymmetrical moment pattern. The actuator and the upper portion of the specimen were connected via the *L*-shaped loading girder. The top block was restrained from rotating via the four-bar mechanism that was connected to the *L*-shaped loading girder. This was performed to simulate typical boundary conditions that are expected in real buildings. Meanwhile, the test specimens were braced laterally to prevent out-of-plane movements.

The specimens were subjected to quasi-static cyclic loading using a displacement-controlled procedure, and the loading system was that the drift ratio θ=1/1200, 1/800, 1/500, 1/400, 1/300, 1/250, 1/200, 1/150, 1/100, 1/80, 1/60, 1/50, 1/40, 1/30, 1/20. One cycle was conducted at each drift level before yielding, and three cycles was conducted at a given drift level to evaluate the degradation of the strength and stiffness of the specimen after the yielding of the specimen. The drift ratio, θ, is defined as the lateral displacement divided by the span of the coupling beam. The specimen was considered to yield when the tensile strain of the longitudinal reinforcement reached the yield strain or when an obvious turning point appeared in the load-displacement curves. The test was stopped when the applied sustainable loads dropped below 85% of the maximum loads.

The horizontal load was measured using a load cell that was installed at the actuator, and the shear in the coupling beam was assumed to be equal to the applied load. Because the readings from the hydraulic actuator were inaccurate due to deformations in the loading system, the horizontal displacement of the specimen that was reached at each drift level was monitored using displacement meters that were placed at the top and bottom of the coupling beam. To monitor the strain and yield status of the reinforcements, strain gauges that were attached to the surface of the bars were installed at selected locations on the longitudinal and transverse reinforcements. The data were collected automatically by the measurement system.
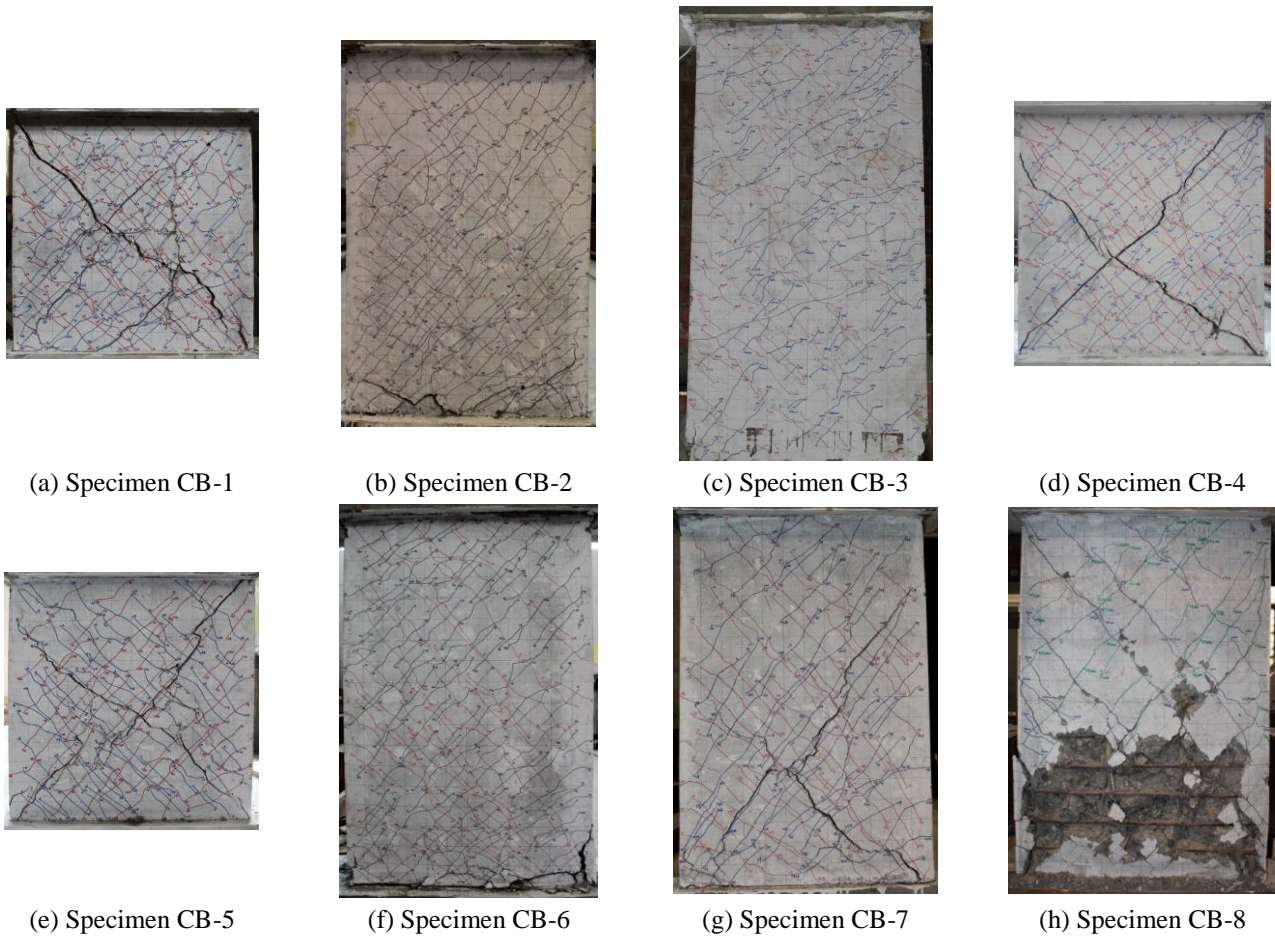
(a) Specimen CB-1   (b) Specimen CB-2   (c) Specimen CB-3   (d) Specimen CB-4

(e) Specimen CB-5   (f) Specimen CB-6   (g) Specimen CB-7   (h) Specimen CB-8

Fig. 4 Crack distribution and failure modes of the specimens

3. Experimental results and analysis

3.1 Cracking and failure modes

The crack distribution and failure modes of each specimen at failure are shown in Fig. 4. The matrix materials of specimens CB-1, CB-4 and CB-5 were FRCC. The span-to-depth ratio and stirrup ratio were 1.0 and 1.12%, respectively, for all three specimens, whereas the FRCC strength varied. The failure process and failure modes of the three specimens under cyclic loading were similar, and specimen CB-1 is used as an example to describe the failure process of the FRCC coupling beam that has a span-to-depth ratio of 1.0. The initial crack appeared at the end of the coupling beam at a load of 133.11 kN, which corresponded to a drift ratio of 0.2%. As the displacement increased, large amounts of new diagonal cracks appeared, and the existing cracks widened. The longitudinal reinforcement yielded at a drift ratio of 1.25%. Simultaneously, a large number of fine micro-cracks appeared around the existing diagonal cracks. The specimen reached the peak load at a drift ratio of 2%. Meanwhile, the corner-to-corner diagonal crack suddenly widened, and the maximum crack width reached 5.5 mm. With the increase in the drift level, the shear strength of the specimen decreased. The existing cracks constantly widened and extended, and there were basically no new cracks. The main

diagonal crack was through the section of the coupling beam, and the maximum diagonal crack width reached 10 mm at a drift ratio of 3.5%. This specimen finally underwent shear failure at a drift ratio of 4%, and the maximum crack width reached 11.5 mm.

The FRCC strength and span-to-depth ratio of specimens CB-2, CB-6 and CB-7 were all the same and were 54.24 MPa and 1.5, respectively. The variable was the stirrup ratio. The failure process and failure modes of the three specimens under cyclic loading were similar. Thus, specimen CB-2 is taken as an example to describe the failure process of the FRCC coupling beam with a span-to-depth ratio of 1.5. For specimen CB-2, the initial diagonal crack appeared at the end of the coupling beam at a load of 110 kN, which corresponded to a drift ratio of 0.24%. The longitudinal reinforcement yielded at a drift ratio of 1.2%. Many new fine cracks appeared, and a slight horizontal crack that was approximately 6 cm in length appeared at the connection of the coupling beam and wall pier. When the drift ratio was 2%, the specimen reached the maximum load. The maximum crack width at the lower end of the coupling beam was 7 mm, and it ran throughout the section of the coupling beams at a drift ratio of 3.6% as the carrying capacity decreased. This specimen finally failed due to the increasing of deformations after the yielding of the longitudinal reinforcements and the loss of shear strength. This failure mode was called shear-flexural failure.

The matrix materials of the specimen CB-3 were FRCC, and the span-to-depth ratio was 2.0. The initial flexural crack appeared at the end of the coupling beam at a load of 120.8 kN, which corresponded to a drift ratio of 0.25%. As the displacement increased, several small flexural cracks appeared in the beam end. The initial diagonal crack appeared in the surface of the coupling beam at a drift ratio of approximately 0.33%. Then, the cracks extended, and the amount of diagonal cracks gradually increased. Because of the good crack control ability of the FRCC material, many small cracks appeared around the existing diagonal cracks, showing a clear multi-crack development. The longitudinal reinforcement of the specimen yielded at a drift ratio of 0.67%, and the development of cracks accelerated as a large number of fine cracks appeared. The load dropped below 85% of the maximum load value at a drift ratio of 2.73%. The specimen lost the carrying capacity at a drift ratio of approximately 4%, and the specimen underwent shear-flexural failure. Additionally, no concrete spalling was observed for any of the FRCC coupling beams throughout the testing.

Specimen CB-8 was an ordinary concrete coupling beam, and the span-to-depth ratio was 1.5. An initial diagonal crack appeared in the lower part of the coupling beam at 200 mm from the wall pier at a load of 115.3 kN, which corresponded to a drift ratio of 0.24%. As the drift level increased, some new diagonal cracks appeared, and the core of the coupling beam was divided into many small pieces. The development of a diagonal crack accelerated, and longitudinal reinforcement yielded at a drift ratio of 1.5%, which was accompanied by the cracking of concrete and a maximum crack width of 1 mm. The specimen reached the maximum load, and the diagonal crack widened to 2 mm at a drift ratio of 2%. As the drift level increased, the concrete cover near the cracks gradually fell off, and the stirrups were exposed. A large area of the concrete in the lower part of the coupling beam fell off at a drift ratio of 3.2%. Then, the specimen lost the carrying capacity and underwent shear failure.

Under the same conditions, the FRCC coupling beam exhibited shear-flexural failure, whereas the concrete coupling beam exhibited shear failure, and the concrete spalling was serious. Contrary to ordinary concrete, FRCC materials exhibit multiple cracking and strain hardening properties, which serves their functions in delaying damage of diagonal tensile cracks. With the increase of the drift level, the tensile stresses across cracks have improved and the occurrence of shear failure is delayed because of the

(a) Specimen CB-1

(b) Specimen CB-2

(c) Specimen CB-3

(d) Specimen CB-4

(e) Specimen CB-5

(f) Specimen CB-6
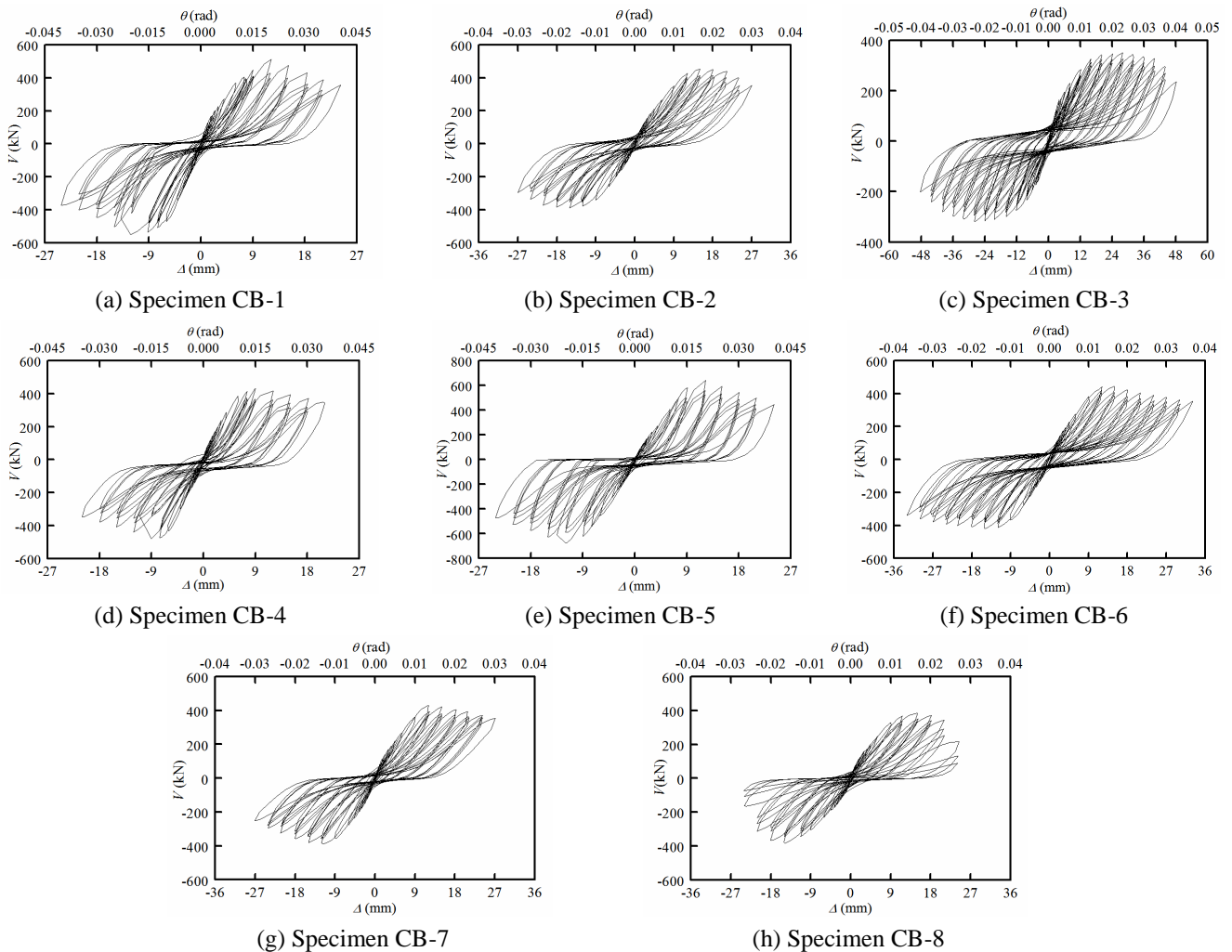
(g) Specimen CB-7

(h) Specimen CB-8

Fig. 5 Hysteretic loops of the specimens

bridging effect of the fibers on the crack interface. Thus, FRCC materials are able to provide confinement and contributing to shear strength of coupling beams with reduction or replacement of the diagonal reinforcements to achieve a stable response under large displacement reversals. For the FRCC coupling beams with different stirrup ratios, the failure modes of the FRCC coupling beams with small span-to-depth ratios changed from shear failure to shear-flexural failure with an increase in the stirrup ratio.

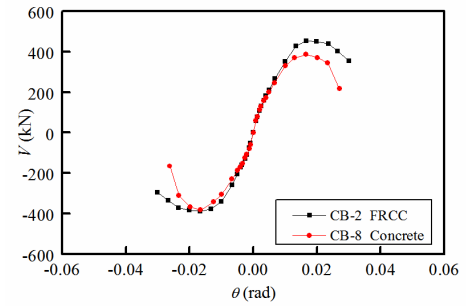### 3.2 Hysteretic curves and skeleton curves

The measured hysteresis and skeleton curves of each specimen are shown in Figs. 5 and 6, respectively. Before reaching the yield state, the load-displacement curve is substantially linear, and the loading curves generally coincide with the unloading ones. With an increase in displacement, the loading curves do not coincide with the unloading ones, and the area of hysteresis loop increases. When the load exceeds the peak load, the slope of the load-displacement curve decreases, and there is degradation in the strength and stiffness. The unloading stiffness decreases as the displacement increases, and a pinching phenomenon appears in the hysteresis curves of each specimen.

Specimens CB-2 and CB-8 have the same reinforcement details and span-to-depth ratio, and only the materials are different. The hysteresis loop area of the ordinary concrete coupling beam (specimen CB-8) is small, and the degradation of the strength and stiffness is obvious. However, the hysteresis curve area of the FRCC coupling beam (specimen CB-2) is larger. Compared with specimen CB-8, the shear capacity of specimen CB-2 increased by 9.71%, and the ultimate displacement corresponding to a 15% drop in load increased by 17.85%, indicating that the energy performance and ductility of coupling beams can be improved by using the FRCC material.
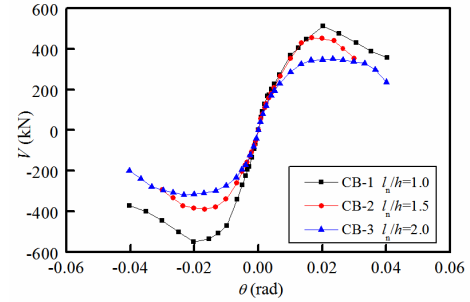
In Figs. 5(a), 5(b), 4(c) and 6(b), the trend of the skeleton curve of each specimen in the ascending branch is approximately the same, and the stiffness during this stage decreases with an increase in the span-to-depth ratio. As the span-to-depth ratio of the specimen increases, the hysteresis loop is fuller, the energy dissipation capacity has been improved, and the shear strength decreases.

The FRCC strength and span-to-depth ratio of specimens CB-6, CB-2 and CB-7 are all the same. The stirrup spacing is 50 mm, 75 mm and 100 mm; the bearing capacities are 432.16 kN, 422.31 kN and 408.14 kN, and the corresponding ultimate displacements are 28.64 mm, 24.55 mm and 23.05 mm, respectively. Thus, the bearing capacity and ultimate displacement increase marginally as the stirrup spacing decreases. When the load exceeds the peak load, the hysteresis cycles of specimen CB-6, which has a larger number of stirrups, significantly increase. Additionally, the stiffness degradation is relatively slow, and the specimen has good deformability.
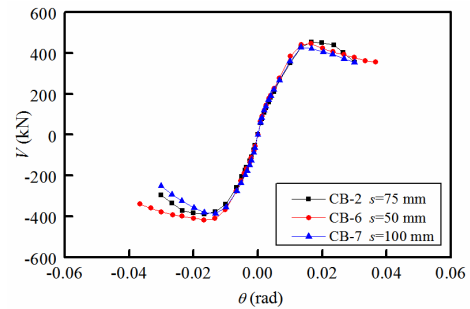
The specimens CB-1, CB-5 and CB-4 have the same span-to-depth ratio of 1.0, which is relatively small. Before reaching the peak load, the stiffness in the ascending branch of the skeleton curve of each specimen increases with an increase in the FRCC strength. There are diagonal cracks in
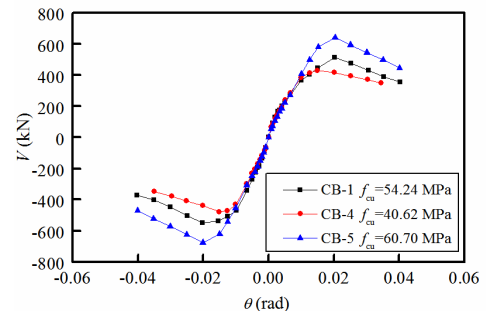

(a) Effect of the matrix material

(b) Effect of the span-to-depth ratio

(c) Effect of the stirrup spacing

(d) Effect of the FRCC strength

Fig. 6 Skeleton curves of the specimens

the specimens as the peak load is reached, but each specimen can continue to carry the load, and the load declines slowly as the displacement increases. Compared with specimen CB-4, the shear strength of specimens CB-1 and CB-5 increased by 16.88% and 44.87%, respectively, indicating that the bearing capacity of the specimens are improved as the FRCC strength increases.

3.3 Shear capacity and ductility

To reflect the deformability of the coupling beam

Table 5 Load and displacement of the specimens at characteristic points

Specimen	loading direction	Yield point			Peak point			Ultimate point			μ	$\bar{\mu}$	λ
		Δ_y (mm)	θ_y (% rad)	V_y (kN)	Δ_m (mm)	θ_m (% rad)	V_m (kN)	Δ_u (mm)	θ_u (% rad)	V_u (kN)			
CB-1	Push	7.82	1.30	413.20	12.16	2.03	512.95	17.99	3.00	436.01	2.30	2.43	0.17
	Pull	-6.66	-1.11	-487.82	-12.18	-2.03	-549.11	-16.97	-2.83	-466.74	2.55		0.18
CB-2	Push	9.16	1.02	354.78	15.01	1.67	454.06	24.86	2.76	385.95	2.71	2.71	0.15
	Pull	-8.96	-1.00	-339.15	-15.01	-1.67	-390.56	-24.25	-2.69	-331.97	2.71		0.13
CB-3	Push	11.92	0.99	282.72	27.98	2.33	350.70	43.79	3.65	298.09	3.67	3.82	0.12
	Pull	-10.31	-0.86	-254.96	-27.93	-2.33	-318.27	-40.94	-3.41	-270.53	3.97		0.11
CB-4	Push	5.85	0.98	378.09	8.98	1.50	429.47	18.80	3.13	365.05	3.21	2.78	0.19
	Pull	-6.51	-1.08	-445.37	-9.02	-1.50	-479.18	-15.25	-2.54	-407.30	2.34		0.21
CB-5	Push	9.62	1.60	589.67	12.23	2.04	640.65	18.08	3.01	544.56	1.88	1.93	0.19
	Pull	-9.06	-1.51	-621.55	-12.04	-2.01	-675.71	-17.96	-2.99	-574.35	1.98		0.20
CB-6	Push	9.77	1.09	396.50	14.90	1.66	445.63	26.76	2.97	378.79	2.74	3.02	0.15
	Pull	-9.27	-1.03	-369.62	-15.03	-1.67	-418.70	-30.53	-3.39	-355.89	3.29		0.14
CB-7	Push	9.65	1.07	374.45	12.01	1.33	428.79	25.29	2.81	364.47	2.62	2.61	0.14
	Pull	-7.98	-0.89	-332.01	-11.84	-1.32	-387.28	-20.81	-2.31	-329.19	2.61		0.13
CB-8	Push	9.35	1.04	334.30	14.93	1.66	386.25	21.44	2.38	328.31	2.29	2.18	0.14
	Pull	-9.75	-1.08	-318.81	-14.85	-1.65	-383.59	-20.23	-2.25	-326.05	2.08		0.14

specimens, the displacement ductility coefficient, $\mu=\Delta_u/\Delta_y$, was used to be the performance indicator. The measured shear-compression ratio, λ, comprehensively reflects the influence of the shear values of a coupling beam, the concrete strength and cross-sectional dimensions on the performance of coupling beams, which can be expressed as $\lambda=V/(f_cbh_0)$, where, V is the peak load V_m of the coupling beam; f_c is the mean value of the prism axial compressive strength, $f_c=0.8f_{cu}$; b is the width of the coupling beam section; h_0 is the effective depth of the coupling beam section, which is the distance from the extreme compression fiber to the centroid of the longitudinal tension reinforcement.

The load, displacement, and drift ratio of each characteristic point of the specimens as well as displacement ductility coefficient and shear-compression ratio that were obtained from the experiment are shown in Table 5. The yield load, V_y, was determined based on the measured load-displacement skeleton curves. The ultimate load, V_u, is the load that declines to 85% of the peak load V_m. $\bar{\mu}$ is the mean value of the displacement ductility coefficient in the positive and negative.

When the reinforcement details and span-to-depth ratio were the same compared with the ordinary concrete coupling beam (specimen CB-8), the yield load, peak load, ultimate displacement and displacement ductility coefficient of the FRCC coupling beam (specimen CB-2) increased by 6.25%, 9.71%, 17.80% and 24.31%, respectively. The drift ratios of the tested FRCC coupling beams at failure are 2.54%~3.65%, which is sufficient for seismic applications according to FEMA 356 (Federal Emergency Management Agency 2000). Because FRCC materials exhibit excellent deformation properties, the shear capacity and deformation capacity of the coupling beams can be improved by using FRCC materials.

The specimens CB-1, CB-2 and CB-3 have the same stirrup ratio and FRCC strength but different span-to-depth ratios, and the displacement ductility coefficients are 2.43, 2.71 and 3.82, respectively. The corresponding shear capacities which are the average peak load determined for the positive and negative directions of loading are 531.03 kN, 422.31 kN, and 334.49 kN, respectively. Compared with the specimen CB-1, the carrying capacity of the specimens CB-2 and CB-3 was reduced by 20.47% and 37.01%, respectively.

When the stirrup ratio and span-to-depth ratio was the same, the shear capacity of specimens CB-5 and CB-1 improved by 44.87% and 16.88%, respectively, compared with specimen CB-4, which has a different FRCC strength, and the corresponding displacement ductility coefficients decreased by 30.58% and 12.59%.

When the FRCC strength and span-to-depth ratio was the same, for the different stirrup ratios, the shear capacity of specimens CB-6 and CB-2 improved by 5.91% and 3.50% compared with that of specimen CB-7, and the displacement ductility coefficients increased by 15.71% and 3.83%, respectively.

The above analysis shows that the span-to-depth ratio, the FRCC strength and the stirrup ratio have an influence on the shear capacity and deformation capacity of coupling beams. As the span-to-depth ratio of the coupling beam increases, the shear capacity decreases, and the displacement ductility coefficient and deformation capacity increase. With an increase in the FRCC strength, the shear capacity of the coupling beam increases, whereas the displacement ductility coefficient and deformation capacity decrease. As the stirrup ratio increases, the shear capacity and deformation capacity increase. The measured shear-compression ratios of the FRCC coupling beam specimens are 0.11 to 0.21, and the corresponding design values of the shear-compression ratios that are calculated by adopting the design values of the concrete axial compressive strength are
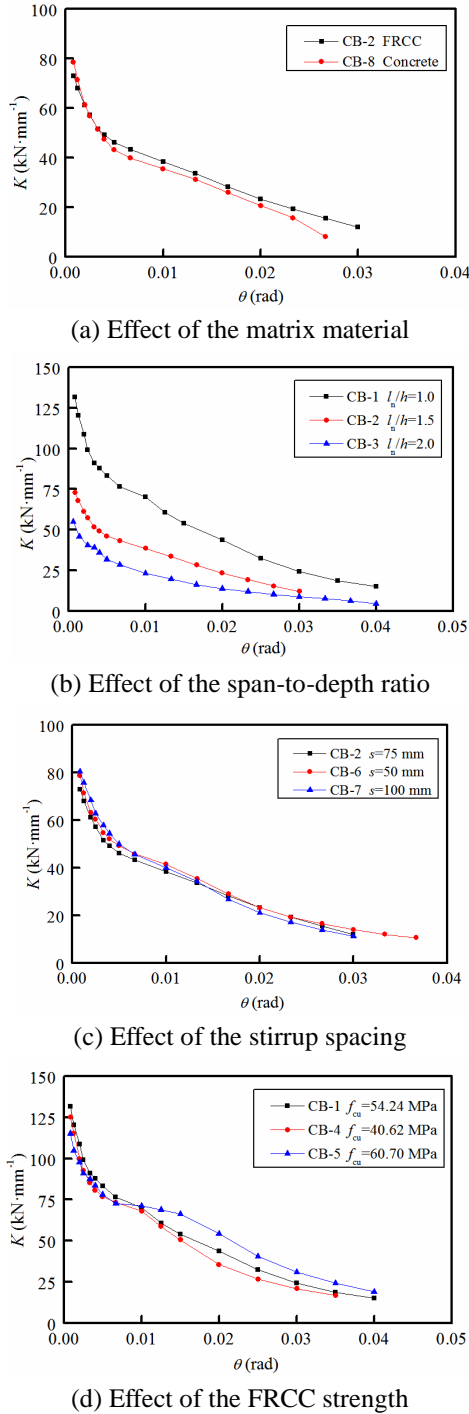
(a) Effect of the matrix material

(b) Effect of the span-to-depth ratio

(c) Effect of the stirrup spacing

(d) Effect of the FRCC strength

Fig. 7 Stiffness degradation curves of the specimens

stiffness degradation curves for each specimen is shown in Fig. 7. The initial stiffness of the ordinary concrete coupling beam was larger than that of the FRCC coupling beams under the same conditions, whereas the stiffness degradation curves of the FRCC coupling beam slowly decreases with an increase in displacement. This is primarily because the elastic modulus of FRCC materials is smaller than that of ordinary concrete, and the initial stiffness of FRCC specimen is small. However, because FRCC materials have a higher tensile strain and pseudo strain-hardening behavior under tension, which improves the tensile strength of the diagonal tension of the coupling beam, the degradation of the stiffness of the coupling beam is slow. As the span-to-depth ratio increases, the initial stiffness of the beam decreases and the rate of degradation decreases even more slightly (Fig. 7(b)), indicating that the span-to-depth ratio has a significant influence on the stiffness of coupling beams. For the different stirrup spacing, the initial stiffness of each specimen is similar, and the stiffness degradation trends are generally similar. However, when the stirrup spacing is smaller, generally, the stiffness degradation curve is less steep (Fig. 7(c)). For the different FRCC strengths, the stiffness and the degradation trend of each specimen is substantially similar at the beginning of the loading. Then, the stiffness and the degradation rates increase with an increase in the FRCC strength, indicating that the FRCC strength has an effect on the stiffness of the coupling beam (Fig. 7(d)).

3.5 Strength degradation

The bearing capacity of coupling beams will decrease with an increase in the number of cycles at the same drift level, and the strength degradation factor for coupling beams is defined as $\eta_i = P_{2,i}/P_{1,i}$, where $P_{1,i}$ and $P_{2,i}$ are the maximum load in the first and second cycles at the i drift level, respectively.

The strength degradation curves of the specimens are provided in Fig. 8. The strength degradation factor of each specimen decreased slowly with an increase in the drift ratio except for specimen CB-8. The strength degradation factor of specimens CB-1, CB-4 and CB-5 at peak load became suddenly small, this is mainly because the span-to-depth ratios of the three specimens were relatively small, thus the diagonal crack width widened when the peak load was reached, and the shear capacity of the specimens significantly decreased in the second cycle, so the strength

0.19 to 0.37. The limitation of design value of shear-compression ratio for coupling beams with small span-to-depth ratios is 0.15 in the code for the design of concrete structures (GB 50010 2010). These results improve the limitation of the shear-compression ratio for coupling beams with small span-to-depth ratios somewhat.

3.4 Stiffness degradation

The secant stiffness was used to calculate the stiffness of the coupling beams at each drift level. A comparison of the
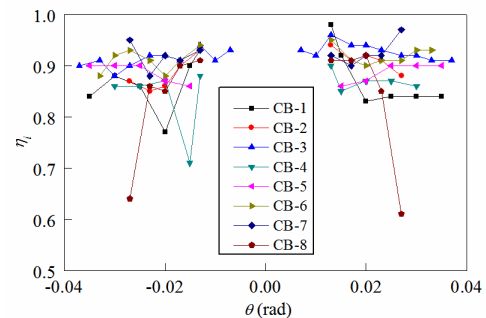

Fig. 8 Strength degradation curves of the specimens

degradation factor was smaller compared with that of other cycles. The strength degradation factors of other FRCC coupling beams were 0.85 to 0.97, and the average value was 0.92. The strength degradation factor of the ordinary concrete coupling beam was 0.61 to 0.92, and the average value was 0.83. The carrying capacity of the FRCC coupling beams that had a sufficient safety reserves degraded slowly throughout the loading process, whereas the carrying capacity of the ordinary concrete coupling beam significantly decreased after the peak load.
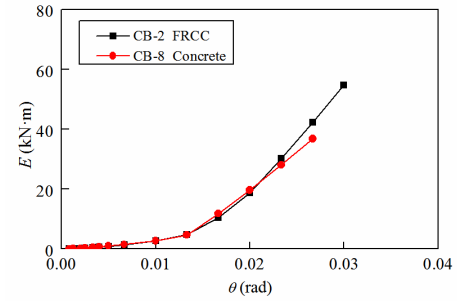
3.6 Energy performance

Energy performance is the ability of members to consume seismic energy, and when the energy performance is stronger, the seismic performance of the members is improved. The energy performance of each coupling beam specimen can be represented by the cumulative energy in repeated horizontal loads. The relationships between the cumulative energy and the drift ratio for each specimen are shown in Fig. 9.

The coupling beam specimen was in the elastic state at the beginning of loading, and the cumulative energy was very small and nearly zero. As the displacement increased, each specimen exhibited inelastic deformation, and the cumulative energy of every specimen increased with an increase in the drift ratio. The cumulative energy of the FRCC coupling beam was 1.15 times that of the ordinary concrete coupling beam at 2.67% drift, showing that the use of FRCC materials in coupling beams can effectively improve the energy dissipation capacity. The cumulative energies of the specimens CB-3 and CB-2 were 2.71 and 1.77 times that of specimen CB-1 at 3% drift, respectively, indicating that when the span-to-depth is larger, the energy consumption is larger. Furthermore, the growth rate of the cumulative energy is larger at higher drift levels. The FRCC strength, cross-sectional dimension and span for specimens CB-2, CB-6 and CB-7 were the same, and only the stirrup spacing was different. The cumulative energies at 1%, 2% and 3% drift increased by 18.18%, 16.83% and 28.81% when the stirrup spacing was reduced from 100 mm (specimen CB-7) to 50 mm (specimen CB-6), respectively, indicating that the closely spaced stirrups can greatly improve the energy performance of the coupling beam. Moreover, the cumulative energy of the coupling beam increased as the FRCC strength increased.
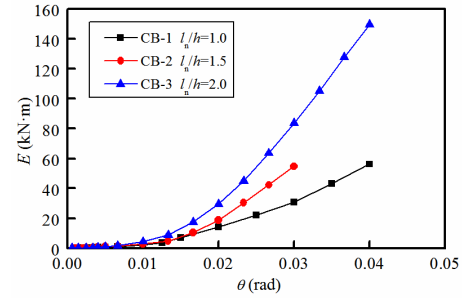
4. Shear strength of the coupling beams

The coupling beam with a small span-to-depth ratio is in the category of deep beams. The action of concrete, stirrups and the contribution of longitudinal reinforcement should be considered with respect to the shear strength of coupling beams. When the span-to-depth ratio is not greater than 2.5, the recommended calculation formula for the shear strength of the coupling beams by Chinese code (GB 50010 2010) is as follows
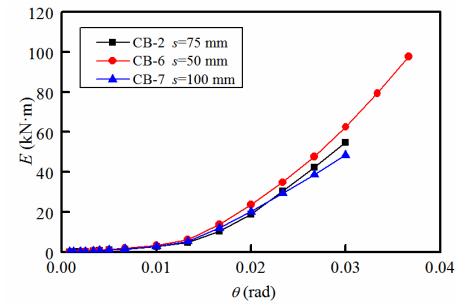
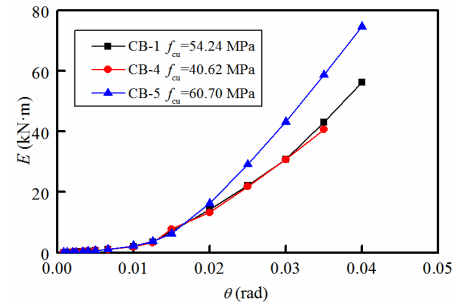$$V = 0.38 f_t b h_0 + 0.9 f_{yv} \frac{A_{sv}}{s} h_0 \tag{1}$$

(a) Effect of the matrix material

(b) Effect of the span-to-depth ratio

(c) Effect of the stirrup spacing

(d) Effect of the FRCC strength

Fig. 9 Energy dissipation curves of the specimens

Experimental research and theoretical analysis show that the span-to-depth ratio has a significant influence on the shear strength of coupling beams (Liang *et al*. 2009; GB 50010 2010). As the span-to-depth ratio decreases, the proportion of concrete and longitudinal reinforcement for the shear strength of the coupling beams increase, and the action of the stirrups weakens. According to a total of 56 tests on coupling beams that all failed in shear (Gong and Fang 1988, Sun *et al*. 1994, Tassios *et al*. 1996, Pi 2008, Zhang *et al*. 2008, Brena and Ihtiyar 2011, Cheng and Su 2011, Ma 2011, Jia 2012, Ye *et al*. 2014), the shear strength of coupling beams with small span-to-depth ratios can be
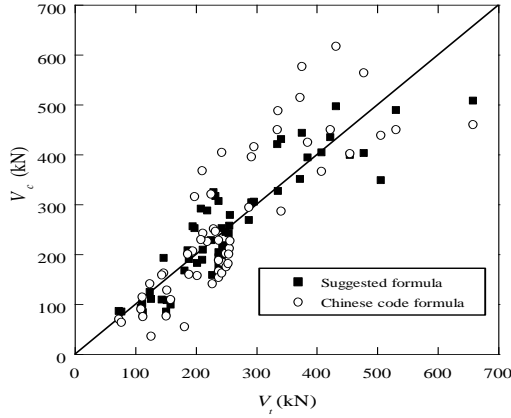
Fig. 10 Comparison of the shear capacities of the coupling beams

calculated based on the above calculation model and statistical regression analysis as follows

$$V = \frac{1.05}{\left(0.5 l_n / h + 1\right)} f_t b h_0 + 0.22 \left(\frac{l_n}{h}\right) f_{yv} \frac{A_{sv}}{s} h_0 + 0.16 \frac{f_y A_s}{\left(l_n / h\right)}$$

(2)

where l_n is the span of the coupling beam, f_t is the tensile strength of the FRCC material or concrete, b is the width of the coupling beam section, h and h_0 are the height and effective height of the coupling beam section, respectively, f_y is the yield strength of the longitudinal reinforcement, A_s is the area of the longitudinal reinforcement, f_{yv} is the yield strength of the stirrups, A_{sv} is the area of stirrups within spacing s, and s is the spacing of the stirrups.

The shear strength of 56 coupling beam specimens that had small span-to-depth ratios were calculated according to Eqs. (1) and (2), and the comparison of the calculated values (V_c) and the experimental values (V_t) is shown in Fig. 10. The average value and coefficient of variation of the ratio of the experimental value to the calculated value according to Eq. (1) are 1.16 and 0.46, respectively. The average value and coefficient of variation of the ratio of the experimental value to the calculated value according to Eq. (2) are 1.06 and 0.22, respectively. The first, second and third terms of Eq. (2) correspond to the concrete, stirrups and longitudinal reinforcement contribution to the shear strength, respectively. The effect of the span-to-depth ratio is considered in all terms. The suggested formula can better evaluate the shear strength of the coupling beams with small span-to-depth ratios compared with that of Chinese code.

For the seven FRCC coupling beams and the concrete coupling beam specimens studied here, the shear strength was calculated according to Eq. (2), and the average value and coefficient of variation for the ratio of the experimental value to the calculated value are 1.02 and 0.15, respectively. Thus, the calculated values obtained according to Eq. (2) are in agreement with the experimental results.

5. Conclusions

Results from a research program that aimed to improve the seismic performance and shear behavior of coupling beams with small span-to-depth ratios through the use of FRCC materials were reported. The following conclusions can be made on the basis of the results of experiment:

• Eight coupling beams with small span-to-depth ratios exhibited shear failure or shear-flexural failure. As the span-to-depth and stirrup ratios increased, the failure mode of the FRCC coupling beams with small span-to-depth ratios was gradually changed from brittle shear failure to shear-flexural failure with a certain ductile characteristics. The carrying capacity of the ordinary concrete coupling beam decreased rapidly after reaching the peak load, and the concrete spalling was serious at failure load. However, because of the fiber bridging in the interface of the cracks, which exhibited a large degree of control on the cracks, the cracks were generally fine. FRCC materials in the FRCC coupling beam specimens did not spall. This suggests that the FRCC coupling beams have good resistance ability to damage and can continue to be used with little repair after a major earthquake, which can reduce or avoid post-earthquake repair costs. It suggests that the FRCC coupling beams with conventional reinforcement can be used in the construction, especially when the width of the coupling beam cross section is small.

• Compared with ordinary concrete coupling beams, the shear strength, ultimate displacement and displacement ductility coefficient of FRCC coupling beams increased by 9.71%, 17.80% and 24.31%, respectively. The cumulative energy of the FRCC coupling beams at 2.67% drift was 1.15 times that of the ordinary concrete coupling beams, and the strength and stiffness degradation was relatively slow, indicating that the use of FRCC materials instead of ordinary concrete in coupling beams can greatly improve the deformation and energy dissipation capacity.

• The span-to-depth ratio, matrix strength and stirrup ratio have a significant impact on the failure mode, deformation, energy dissipation capacity, stiffness and strength degradation of coupling beams. With a decrease in the span-to-depth ratio and an increase in the FRCC strength, the shear strength of coupling beams increases, whereas the displacement ductility coefficient and deformation capacity decrease. Moreover, as the stirrup ratio increases, the carrying capacity, deformation and energy consumption capacity increase.

• The measured value of shear-compression ratio of seven FRCC coupling beams was from 0.11 to 0.21, corresponding to the design value of shear-compression ratio was from 0.19 to 0.37. Thus, the limitation of the shear-compression ratio has been improved for coupling beams that have a span-to-depth ratio of less than 2.5.

• The suggested shear strength formula for coupling beams that the span-to-depth ratio is not greater than 2.5 considers the impact of the span-to-depth ratio, stirrups and longitudinal reinforcement, and the calculated results are in good agreement with the experimental results.

Acknowledgements

References

ACI 318 (2014), Building Code Requirements for Structural Concrete and Commentary (ACI 318-14), American Concrete Institute, Farmington Hills, MI.

Brena, F.S. and Ihtiyar, O. (2011), "Performance of conventionally reinforced coupling beams subjected to cyclic loading", *J. Struct. Eng.*, **137**(6), 665-676.

Canbolat, B.A., Parra-Montesinos, G.J. and Wight, J.K. (2005), "Experimental study on seismic behavior of high-performance fiber-reinforced cement composite coupling beams", *ACI Struct. J.*, **102**(1), 159-166.

Cheng, B. and Su, R.K. (2011), "Retrofit of deep concrete coupling beams by a laterally restrained side plate", *J. Struct. Eng.*, **137**(4), 503-512.

Federal Emergency Management Agency. (2000), "Prestandard and commentary for the seismic rehabilitation of buildings", Research Report No. FEMA 356, Federal Emergency Management Agency, Washington, D.C.

Fischer, G. and Li, V.C. (2002), "Effect of matrix ductility on deformation behavior of steel-reinforced ECC flexural members under reversed cyclic loading conditions", *ACI Struct. J.*, **99**(6), 781-790.

Fischer, G. and Li, V.C. (2003), "Deformation behavior of fiber-reinforced polymer reinforced engineered cementitious composite (ECC) flexural members under reversed cyclic loading conditions", *ACI Struct. J.*, **100**(1), 25-35.

Foltz, R.R., Lee, D.H. and LaFave, J.M. (2017), "Biaxial behavior of high-performance fiber-reinforced cementitious composite plates", *Constr. Build. Mater.*, **143**, 501-514.

Fortney, P.J., Rassati, G.A. and Shahrooz, B.M. (2008), "Investigation on effect of transverse reinforcement on performance of diagonally reinforced coupling beams", *ACI Struct. J.*, **105**(6), 781-788.

Galano, L. and Vignoli, A. (2000), "Seismic behavior of short coupling beams with different reinforcement layouts", *ACI Struct. J.*, **97**(6), 876-885.

GB 50010 (2010), Code for Design of Concrete Structures (GB 50010-2010), Ministry of Housing and Urban-Rural Development of the People's Republic of China, Beijing.

Gong, B. and Shahrooz, B.M. (2001), "Steel-concrete composite coupling beams-behavior and design", *Eng. Struct.*, **23**(11), 1480-1490.

Gong, B.N. and Fang, E.H. (1988), "Behavior of reinforced concrete coupling beams between shear walls under cyclic loading", *J. Build. Struct.*, **9**(1), 34-41.

Han, S.W., Lee, C.S., Shin, M. and Lee, K. (2015), "Cyclic performance of precast coupling beams with bundled diagonal reinforcement", *Eng. Struct.*, **93**, 142-151.

Harries, K.A., Gong, B. and Shahrooz, B.M. (2000), "Behavior and design of reinforced concrete, steel, and steel-concrete coupling beams", *Earthq. Spectra*, **16**(4), 775-799.

Jia, B. (2012), "Experimental study on steel fiber reinforced concrete coupling beams with different strengths", Master Dissertation, Zhengzhou University, Zhengzhou.

Kanda, T., Lin, Z. and Li, V.C. (2000), "Tensile stress-strain modeling of pseudostrain hardening cementitious composites", *J. Mater. Civil Eng.*, **12**(2), 147-156.

Khan, M.I. and Abbass, W. (2016), "Flexural behavior of high-strength concrete beams reinforced with a strain hardening cement-based composite layer", *Constr. Build. Mater.*, **125**, 927-935.

Lequesne, R.D., Parra-Montesinos, G.J. and Wight, J.K. (2013), "Seismic behavior and detailing of high-performance fiber-reinforced concrete coupling beams and coupled wall systems", *J. Struct. Eng.*, **139**(8), 1362-1370.

Lequesne, R.D., Parra-Montesinos, G.J. and Wight, J.K. (2016). "Seismic response of fiber-reinforced coupled walls", *ACI Struct. J.*, **113**(3), 435-445.

Li, V.C. and Kanda, T. (1998), "Engineered cementitious composites for structural applications", *J. Mater. Civil Eng.*, **10**(2), 66-69.

Li, V.C., Wang, S. and Wu, C. (2001), "Tensile strain-hardening behavior of polyvinyl alcohol engineered cementitious composite (PVA-ECC)", *ACI Mater. J.*, **98**(6), 483-492.

Liang, X.W., Li, F.Y., Zhang, T. and Deng M.K. (2009), "Experimental study on seismic behavior of new reinforcement scheme deep coupling beams", *Eng. Mech.*, **26**(12), 119-126.

Ma, X. (2011), "Experimental study on reinforced concrete coupling beams with different volume fraction of steel fibers", Master Dissertation, Zhengzhou University, Zhengzhou.

Park, W. and Yun, H. (2011), "Seismic performance of pseudo strain-hardening cementitious composite coupling beams with different reinforcement details", *Compos. Part B Eng.*, **42**(6), 1427-1445.

Paulay, T. and Binney, J.R. (1974), "Diagonally reinforced coupling beams of shear walls", *ACI Spec. Publ.*, **42**(2), 579-598.

Pi, T.X. (2008), "Experimental study on seismic behavior and design method study of small span-to-depth ratio coupling beams of seismic RC shear walls", Ph.D. Dissertation, Chongqing University, Chongqing.

Shin, M., Gwon, S., Lee, K., Han, S.W. and Jo, Y.W. (2014), "Effectiveness of high performance fiber-reinforced cement composites in slender coupling beams", *Constr. Build. Mater.*, **68**, 476-490.

Sun, Z.G., Lin, Z.F. and Dai, R.T. (1994), "Behavior of coupling beams of shear wall reinforced with inclined rhomboidal bars", *J. Build. Struct.*, **15**(5), 14-23.

Tassios, T.P., Moretti, M. and Bezas, A. (1996), "On the behavior and ductility of reinforced concrete coupling beams of shear walls", *ACI Struct. J.*, **93**(6), 711-720.

Ye, Y.X., Qin, L.H., Liu, T. and Sun, X.Y. (2014), "Experimental study on seismic performance of small span-to-depth ratio coupling beams with PVA fiber reinforced concrete", *Appl. Mech. Mater.*, **513**, 134-137.

Zhang, H.Z., Zhang, R.J. and Huang, C.K. (2008), "Experimental study of shear resistance of steel fiber reinforced high-strength concrete coupling beams", *China Civil Eng. J.*, **40**(11), 15-22.

KT